2024

A New Approach for Discriminating Spatially Acquired SERS Spectra Using Antiretroviral Drug Emtricitabine as a Test Sample

Jana Hrncirova
Old Dominion University

Marguerite R. Butler
Old Dominion University, mbutl009@odu.edu

Meredith R. Clark
Eastern Virginia Medical School

Gustavo F. Doncel
Eastern Virginia Medical School

John B. Cooper
Old Dominion University, jcooper@odu.edu

RESEARCH ARTICLE

Journal of RAMAN SPECTROSCOPY WILEY

A new approach for discriminating spatially acquired SERS spectra using antiretroviral drug emtricitabine as a test sample

Jana Hrncirova[1,2] | Marguerite R. Butler[1] | Meredith R. Clark[3] |
Gustavo F. Doncel[3] | John B. Cooper[1]

[1]Department of Chemistry and Biochemistry, Old Dominion University, Norfolk, Virginia, USA

[2]Department of Physical and Macromolecular Chemistry, Faculty of Science, Charles University in Prague, Prague 2, Czech Republic

[3]CONRAD, Department of Obstetrics and Gynecology, Eastern Virginia Medical School, Norfolk, Virginia, USA

Correspondence
J.B. Cooper, Department of Chemistry and Biochemistry, Old Dominion University, 4541 Hampton Boulevard, Norfolk, VA 23529-0126, USA.
Email: jcooper@odu.edu

Abstract

In this study, an antiretroviral drug emtricitabine (also known as FTC or Emtriva) was detected and quantified down to 40 ng/ml by using surface-enhanced Raman spectroscopy (SERS). Its aqueous standards were tested with two types of silver nanoparticles (colloidal and dendritic) using a specially developed aluminum well plate. The SERS spectra were acquired using a Raman scanning device with 30-μm spatial resolution. The spectral data were analyzed using a new approach for the discrimination of the spatially acquired spectra based on the Quality index (Qi). After the Qi is calculated, the spectral data are sorted based on the Qi. This is followed by selecting only the spectra with a high Qi index and comparing the average of all the spatially acquired spectra. This results in an improvement in the spectral signal-to-noise and higher analytical sensitivity of the built calibration curves.

KEYWORDS

antiretroviral drug, emtricitabine, scanning Raman device, surface-enhanced Raman spectroscopy

1 | INTRODUCTION

Human immunodeficiency virus (HIV) is still at the forefront of scientific interest. Despite many years of medical research and progress, no effective therapy is available. The number of people suffering from HIV was 38.4 million, and 1.5 million became newly infected in 2021.[1,2] Currently, the only available antiretroviral therapy is based on HIV drugs treatment.[3–5]

There are a total of seven classes of HIV drugs, and emtricitabine (as well as, e.g., HIV drugs lamivudine, tenofovir disoproxil, or tenofovir alafenamide fumarate) belongs to the class of Nucleoside reverse transcriptase inhibitors.[4–6]

Emtricitabine, commonly abbreviated as FTC, is a synthetic nucleoside analog with activity against human immunodeficiency virus type 1 (HIV-1) reverse transcriptase. Emtricitabine is the (−) enantiomer of a thio-analog of cytidine, whose chemical name is 5- fluoro-1-(2R,5S)-[2-(hydroxymethyl)-1,3-oxathiolan-5-yl]cytosine, and it is typically prescribed in addition to other antiviral drug or drugs for antiretroviral therapy to both treat and prevent HIV-1 infection.[7,8] Adherence to daily pill intake is critical to the success of the therapy but also for preventing

the emergence of difficult-to-treat resistant viral mutants.[2] Objective measures of adherence are therefore an important clinical tool to ensure success in the treatment and prevention of the disease but represent a gap in the field.[9,10] The ultimate goal of our work is to develop a point-of-care test for the detection and quantification of antiviral drugs such as emtricitabine in biological matrices.

Surface-enhanced Raman spectroscopy (SERS) techniques have been applied to pharmaceutical detection and quantification due to their great analytical sensitivity.[11–14] For example, SERS sensors using Au substrates deposited on glass supports, developed by Zanchi et al.[15] in 2020, allowed the detection of the antiepileptic drug Perampanel. Also, a detection method by SERS for low concentrations of the antibiotic drug penicillin G has also been developed and more.[16–23] In literature, the leading methods of detection and quantification of emtricitabine with respect to therapeutic drug monitoring include UPLC, HPLC, and LC-MS/MS.[24–26] A communication published in 2022 proposed optimized HPLC conditions for the identification of emtricitabine and tenofovir, active compounds for analysis in quality control laboratories.[27] Because of its ability to generate unique vibrational signatures specific to individual molecules while only using a small sample volume, SERS offers an alternative approach to detect emtricitabine and other HIV drugs with specificity and at low quantifiable detection limits.

However, the use of colloids to generate SERS imposes limitations on detection, as the surface concentration is in equilibrium with the solution concentration as dictated by the relevant isotherm. Alternatively, the ability to evaporate a colloidal solution to dryness offers the ability to dramatically enhance the quantifiable detection limit by eliminating the solution phase of the analyte and maximizing surface adsorption and hence the resulting SERS signal.[28,29] Unfortunately, this always results in an extremely large degree of spatial heterogeneity with respect to the SERS enhancement. The result is a high degree of irreproducibility, which is dependent on both laser sampling and substrate preparation. One way around this is to prepare highly ordered SERS substrate surfaces in an effort to maximize homogeneity upon sample evaporation.[30,31] Unfortunately, these substrates are expensive and difficult to prepare and/or have limited lifetimes. This contrasts with silver colloids, which are inexpensive and simple to prepare (they are typically synthesized by reduction of silver nitrate with sodium citrate, sodium borohydride, EDTA, or by hydroxylamine hydrochloride).[32–35]

In this work, we use emtricitabine as our model HIV drug, along with two types of silver nanoparticles. Suspensions containing aqueous standards of emtricitabine mixed or deposited on the SERS-active silver nanoparticles are evaporated to dryness on an aluminum well plate, which exhibits no background signal interference. Although the resulting SERS substrate is highly heterogeneous, we show that the combination of the spatially resolved spectral acquisition, along with simple statistical analysis, allows for reproducible results with outstanding limits of quantitation and dramatic enhancement in analytical sensitivity. The introduced methodology in combination with the Raman scanning device could be easily applied to structurally similar molecules or drugs.

2 | EXPERIMENTAL

2.1 | Materials and instrumentation

Hydroxylamine hydrochloride ($NH_2OH \cdot HCl$), hydroxylamine (NH_2OH), silver nitrate ($AgNO_3$), NaOH, and emtricitabine certified secondary pharmaceutical standard were purchased from Sigma-Aldrich. HPLC grade methanol was purchased from Fisher Scientific, and perchloric acid ($HClO_4$) was purchased from J.T. Baker. Milli-Q water (>18.0 MΩ·cm^{-1}) was obtained by purifying deionized water using a Millipore Milli-Q gradient system.

A Wasatch Photonics 785 nm Raman spectrometer with single-stage TEC cooled CCD detector was used for acquisition of all spectra presented in the preceding sections. The scanning device includes a Wasatch Raman Spectrometer attached to an XY Stage and was used for the acquisition of spatially resolved spectra (the scheme of the instrument was previously published).[36] In a typical experiment, samples are placed in each of the 40 wells of the 5×8 aluminum well-plate (manufactured from 1,100-grade aluminum) placed in the computer-controlled scanning device and scanned utilizing software written using National Instruments Labview. For each sample well, the laser is scanned in the square raster pattern, which consists of a series of x-axis line scans that are separated by 354 μm. The spectra are collected at a constant scan velocity 37 μm/s with a fixed spectral integration time 800 ms, laser power 15 mw, and spatial resolution R_x 30 μm. The total acquisition time per sample well is 24.5 min, resulting in a total of 1,806 collected spectra from one sample well.

The aluminum well plate was cleaned by soaking in 50 ml of 1 M NaOH for 2 min, rinsed with deionized water, soaked in a fresh 50 ml of 1 M NaOH solution for 2 min again, rinsed with deionized water, and placed in a fume hood until dried. Next, two drops of $HClO_4$ were deposited in each well and left to sit for 6 min, followed

by rinsing the plate with deionized water and placing it in a fume hood until dried.

SEM imaging was performed using Phenom™ XL G2 Desktop SEM. All micrographs are back-scattered secondary electron (BSE) images taken at an accelerating voltage of 30 kV. A Scientific Evolution 201 UV-Visible Spectrophotometer was used to characterize Ag colloidal nanoparticles.

2.2 | Synthesis of Ag nanoparticles

Prior to synthesis, all glassware was cleaned with aquaregia, rinsed with deionized water, and then rinsed with Milli-Q water.

The synthesis of Ag colloidal nanoparticles was performed following the procedure as described by Leopold and Lendl.[33] Briefly, 0.3 ml of 1 M NaOH was added to 90 ml of $1.6 \cdot 10^{-3}$ M $NH_2OH \cdot HCl$. This mixture was stirred on a magnetic stirrer whose speed of rotation was set to 360 rpm. A 10 ml volume of $1 \cdot 10^{-2}$ M $AgNO_3$ was then added dropwise. The synthesis was stirred for 45 min to completion. The UV-Visible spectrum and SEM images of the Ag colloidal nanoparticles are shown in Figure S1.

The synthesis of Ag dendrites nanoparticles was adapted from Butler et al.[37] The reaction vessel was resting on a submerged compressed air driven magnetic stirrer with a regulated pressure in a thermally stabilized water bath at 25.6°C. Forty milliliters of Milli-Q-water (after the temperature was equilibrated) was mixed with 2 ml of 100 mM $AgNO_3$, followed by dropwise addition of 2 ml of 200 mM NH_2OH. The reaction mixture was let stirring for 15 min. Then, the excess solvent was removed from the reaction solution and replaced by 10 ml of methanol as a washing solvent and sonicated for 5 min. After centrifuging it for 5 min at 3,000 rpm and 25°C, the supernatant was removed, replaced by 10 ml of methanol, vortexed for 30 s, and then centrifuged again. This cleaning process was done three times. Finally, the dendritic nanoparticles were resuspended in 10 ml of methanol (SEM images of the synthesis are displayed in Figure S2).

2.3 | Preparation and deposition of the samples for the experiments on the aluminum well-plates

Seven samples and a blank of emtricitabine with different concentrations were prepared (500, 400, 300, 200, 100, 50, and 40 ng/ml) by dissolving powder emtricitabine certified secondary pharmaceutical standard in Milli-Q-water. Next, 55 μl of analyte was added to 55 μl

Ag nanoparticle solution and vortexed for 3 s. This mixture was then incubated for 1 h in the absence of light. Finally, 20 μl of this reaction solution was deposited in a well on the plate and allowed to evaporate to dryness in the fume hood. Each concentration was deposited in five wells (an entire column). The deposition diagram is displayed in Table S1.

During the deposition of analyte using Ag dendrites nanoparticles, the aluminum well plate was placed on a hot plate set to 40°C, and 20 μl of Ag dendrites nanoparticles solution (sonicated for 3 s prior to deposition) was deposited in each well and allowed them to dry. Seven samples and a blank of emtricitabine with different concentrations were prepared (100,000, 10,000, 2,000, 1,000, 500, 100, and 50 ng/ml). First, 5 μl of methanol was deposited in the well followed by a deposition of 5 μl of the analyte and allowed to dry in a fume hood. Each concentration was deposited in five wells (an entire column). The deposition diagram is displayed in Table S9.

2.4 | Data analysis

Since a large spectral dataset was acquired (a total of 1,806 spectra were acquired for each well) with an extreme degree of heterogeneity in spectral signal-to-noise across each concentration ranging from no emtricitabine signal for a significant majority of spectra to extremely high emtricitabine signal-to-noise for a small minority of spectra, a figure-of-merit or Quality index (Q_i) was calculated (see Equation (1)) and assigned to each spectrum in order to rank the spectral data.

$$Qi = \left[\frac{1}{2n+1} \left(\sum_{j=p-n}^{p+n} I_j - \sum_{j=b_1-n}^{b_1+n} I_j \right) \left(\sum_{j=p-n}^{p+n} I_j - \sum_{j=b_2-n}^{b_2+n} I_j \right) \right]$$
$$\left\{ Q = +\Re, if \left(\sum Ij - \sum Ij \right) < 0 \ 0 \right\}$$
(1)

In Equation (1), p is the position of the peak selected for Q_i, b_1 is a peak baseline position on one side of the peak, b_2 is a peak baseline position on the opposing side of the peak, j is a spectral cm^{-1} index, I_j is the SERS intensity at index j, and $2n + 1$ is the number of j positions averaged (typically 3–5).

Although the exact definition of Q_i is not critical (e.g., in this case, it is simply based on the most intense emtricitabine peak intensity with dual baseline correction and $2n + 1$-point intensity averaging, but it could easily be expanded to multiple peaks or simplified to a single point-baseline), it is important that it reflects intensity *correlated* with emtricitabine enhancement and not just raw intensity, since several spatial positions give rise to
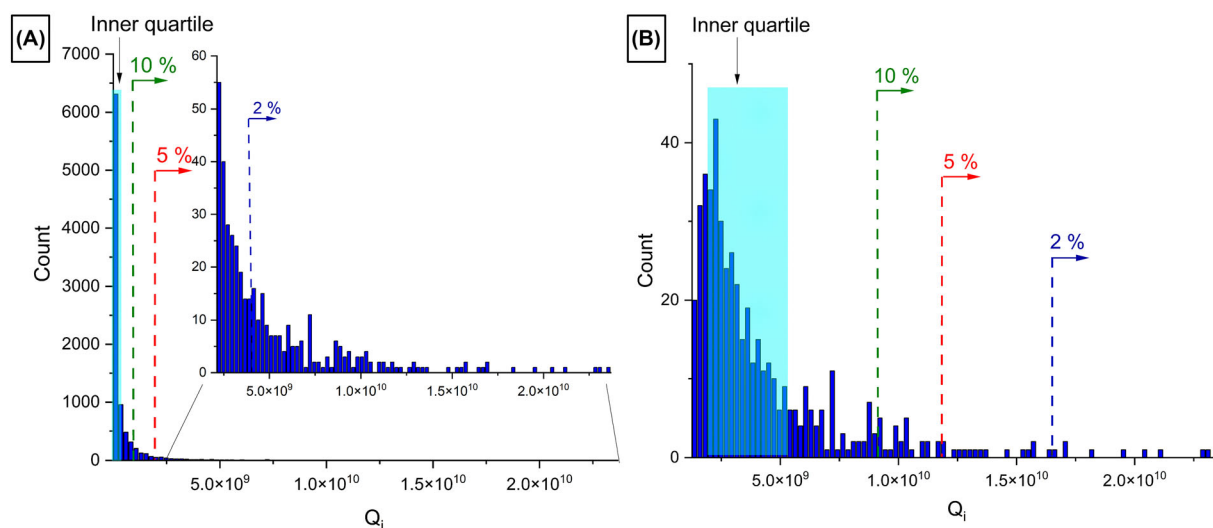
FIGURE 1 Histograms displaying the spectra count with specific Qi values calculated using (A) all and (B) the top 100 Qi-ranked spatially acquired spectra for the wells at a concentration of 500 ng/ml of emtricitabine using Ag colloidal nanoparticles. The inner quartile, the top 10%, 5%, and 2% distributions based on the Qi, is highlighted. For clarity, the inset enlarges the 2% distribution.

high intensity backgrounds due to the background signal. Due to the automated calculation and assignment of the Qi, the process is very fast. This approach is also universal for any large spectral data set since an arbitrary peak, or peaks could be chosen for the Qi analysis and was previously published.[37]

3 | RESULTS AND DISCUSSION

3.1 | Data obtained by using Ag colloidal nanoparticles

For the spectral data acquired by using Ag colloidal nanoparticles, the peak of emtricitabine at 794 cm^{-1} was chosen for the Qi data analysis as the most prominent peak even for the low concentrations without any background interferences.

An efficient way to observe the extreme heterogeneity of spectral data of one concentration (9,030 individual spectra) is to create a histogram using all spectral data by plotting the count of spectra with certain Q_i values. A histogram of this type is shown in Figure 1A using all spatial positions for the 500 ng/ml concentration wells. As observed, the majority of spectra have low values of the Qi, which means negligible SERS emtricitabine enhancement. Indicated on the histogram are the inner quartile distribution (centered not far from $Q_i = 0$) and the top 10%, 5%, and 2% distributions as a function of Qi. The extreme concavity of all the distributions is clearly indicative of a power law distribution. In the 2% distribution (Figure 1A inset), all included spectra correspond to
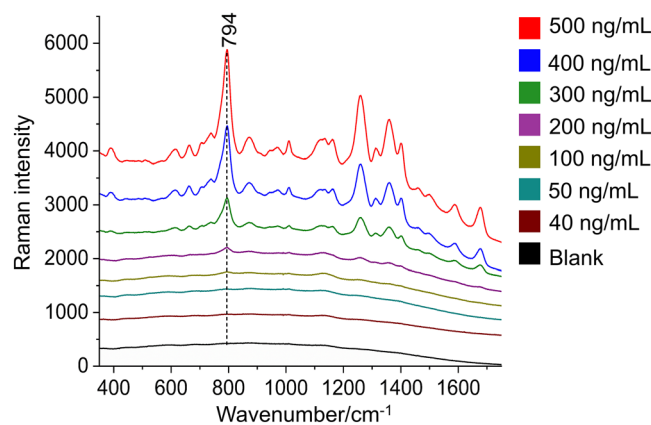

FIGURE 2 The average spectrum from five replicates for each measured concentration of emtricitabine was obtained using all spatially acquired spectra by using Ag colloidal nanoparticles (measured at the excitation wavelength with $\lambda_{exc} = 785$ nm and a laser power of 15 mW).

those with very high signal-to-noise ratios. Additional histograms using all spatial positions for the 400, 300, 200, 100, 50, and 40 ng/ml concentrations wells are shown in Figures S3–S8.

A second type of histogram was constructed, Figure 1B, but this time, only the top 100 Qi-ranked spectra from each well, with a selected concentration, were included. In this case, the power law of the distribution does not appear until slightly inside of the quartile distribution with the top 10%, 5%, and 2% of the distribution occurring at the tailing of the power law (i.e., with no further evidence of significant distribution order in those ranges). These later ranges represent the range of the
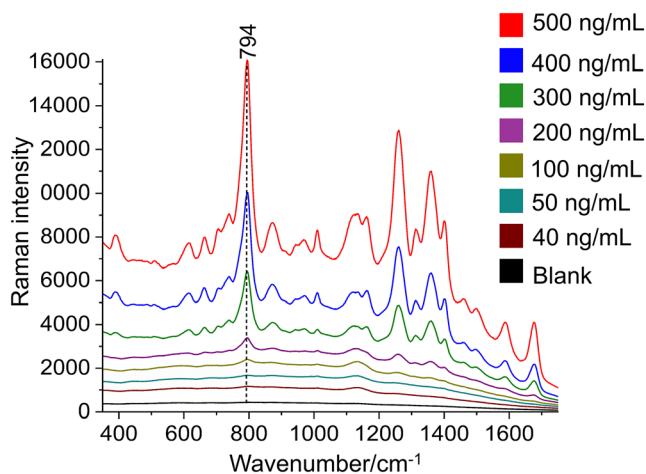
FIGURE 3 The average spectrum from five replicates for each measured concentration of emtricitabine was obtained using the top 100 highest Qi-ranked spatially acquired spectra from each well by using Ag colloidal nanoparticles (measured at the excitation wavelength with λ_{exc} = 785 nm and a laser power of 15 mW).

most intense SERS enhancement hotspots, and as can be seen, these ranges also represent the greatest enhancement variance. Indeed, the top 2% distribution accounts for only 10 samples yet exhibits the widest distribution within the Qi range per sample. These results indicate that although the greatest signal-to-noise ratio is clearly represented by the higher ranges, these ranges also exhibit the greatest variance in signal. Histograms using only the top 100 Qi-ranked spectra from each well for the 400, 300, 200, 100, 50, and 40 ng/ml concentrations wells are shown in Figures S9–S14.

Figure 2 displays the average of spatially acquired spectra as a function of the emtricitabine concentration. Each spectrum represents an average of all spatially acquired spectra (for a given concentration). The spectra for concentrations 100, 50, 40 ng/ml and blank are individually shown in Figures S15–S18 for clarity.

The nature of the spectral background is a consequence of residual impurities from the synthesis and fluorescence. However, for the building of the calibration curves presented in the following text, only the height of the peak at 794 cm^{-1} (or the peak at 786 cm^{-1}, when the Ag dendrites nanoparticles were used) relative to the baseline was utilized.

In comparison, Figure 3 represents spectra as a function of emtricitabine concentration using the special discrimination based on the Qi. First, only the top 100 Qi-ranked spectra from each well were selected. Since five wells were utilized for each well, each spectrum in Figure 3 shows an average of 500 spectra. The spectra for concentrations 100, 50, 40 ng/ml and blank are individually shown in Figures S19–S22. The

elimination of spectra from spatial positions that do not contain significant emtricitabine SERS intensity, as indicated by ranked Qi, was further applied. Figures S23–S26 show spectra representing the top 10%, 5%, 2%, and inner-quartile Q_i distributions from the 100 highest Q_i ranked spectra for each well. As clearly observed in Figure 3, and as intuitively expected, the elimination of spectra from spatial positions that do not contain significant emtricitabine SERS intensity, as represented by ranked Qi, results in a significant increase of signal-to-noise at all concentrations, resulting in a prominent improvement in the detection limit and in the calibration curves in term of the spread of values for each concentration replicate, as shown in the following text.

A series of calibration curves was constructed with varying degrees of spatially resolved spectral discrimination. For all these plots, the concentration is plotted against the baseline corrected intensity of the emtricitabine peak at 794 cm^{-1}, and error bars are included showing the standard deviation of the average spectral intensity of the 794 cm^{-1} peak in each of the five concentration wells, along with a data point showing the mean result for the wells. Here, the calibration plot built using all spatially acquired spectra (from Figure 2) and calibration curve using only the top 100 Qi-ranked spatially acquired spectra from each well (from Figure 3) are compared and shown in Figure 4A,B, respectively. The calibration curves constructed using the top 10%, 5%, 2%, and inner-quartile Q_i distributions of spectra out of the top 100 Qi-ranked spatially acquired spectra are given in Figures S27–S36, and Tables S2–S7 summarized the details about the linear regression.

As can be observed when comparing the results in Figure 4A,B, spatial discrimination based on the Qi results in an improved separation between concentration classes. At low concentrations (insets for both figures), there is a significant improvement in analytical sensitivity (i.e., the slope of the curve) while maintaining a superior separation in classes, especially when compared to the blank. This is indicative of the significant improvement in signal-to-noise being accomplished without a substantial increase in variance among the individual spectra. Relative to the top 100 distribution, the top 10% distribution is comparable, while the inner quartile, the 5% and 2% distributions show a slight degradation in calibration performance. All data sets follow polynomial function (order 3). Nevertheless, there is a noticeable linear trend in the region of the higher concentrations (500–200 ng/ml) and in the region of the lower concentrations (100–0 ng/ml). These two regions were individually fitted with the linear regression to effectively compare the analytical sensitivity between the two regions and across the
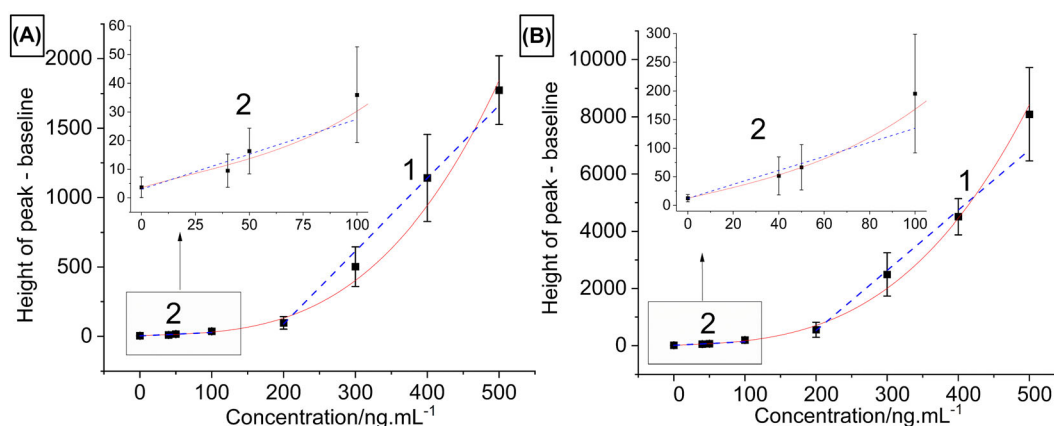
FIGURE 4 Calibration curves constructed based on the peak height at 794 cm^{-1} relative to the baseline calculated from the spectrum obtained using (A) all data and (B) the top 100 Qi-ranked spatially acquired data from each well. Error bars represent the standard deviation from each replicate. The calibration curves were fitted with a polynomial function of order 3 (a red line). Different segments of the data sets were fitted with a linear regression (blue dashed lines). The details about fits are summarized in Table S8.

different Qi-spatial discrimination methods (see Table S8 for details about the linear regression).

Also included in Table S8 are the relative standard deviations (RSD) of each concentration for each discrimination method. By comparing both the slopes and the RSD values of the methods in the two concentration ranges, the spatial discrimination using the Qi results in a dramatic enhancement of the analytical sensitivity ($>5\times$), while also improving the precision reflected by the RSD values. The best selection in terms of the analytical sensitivity is the 2% from the top 100 Qi-ranked spatially acquired data, for the higher concentration range, and the 5% from the top 100 Qi-ranked spatially acquired data, for the lower concentration range. Overall, the higher concentration range shows improvement when comparing all data and the top 100 Qi-ranked spatially acquired data. A slight increase of the RSD values could be seen when comparing the top 100 Qi-ranked spatially acquired data to the top 10%, 5%, and 2% out of the 100 Qi-ranked spatially acquired data. The lower concentration range shows improvement when comparing all data and the top 100 Qi-ranked spatially acquired data, but in case of the top 10%, 5%, and 2% from the 100-Qi ranked spatially acquired data, the RSD values increase and, for the 10% and 5%, are even higher than for all data. Looking at the individual RSD values for 40 ng/ml, as the limit of quantification using Ag colloidal nanoparticles, they increased, but then, they dropped down when the 2% out of the 100 Qi-ranked spatially acquired data are selected. Despite the improvement of the RSD values with a different selection, the RSD values remain around a similar value, which points out at a good reproducibility, and it is consistent with the spherical nature of the nanoparticles and their efficient

packing distribution upon the evaporation in the aluminum wells.

The results displayed to this point are all based on the use of the Ag colloidal nanoparticles with spherical shape and with a uniform size distribution (as reflected in Figure S1). The spherical nature of these particles and their uniform size distribution are expected to result in similar and efficient packing distributions upon the evaporation in the aluminum wells, which, in turn, is expected to result in a more uniform distribution in hotspots. In the following section, these results are compared to those obtained using the Ag dendrites nanoparticles, which are expected to have a more heterogeneous distribution due to their geometries.

3.2 | Data obtained by using Ag dendrites nanoparticles

For the spectral data acquired using Ag dendrites nanoparticles, the peak of emtricitabine at 786 cm^{-1} was chosen for the Qi data analysis as the most prominent peak, even for the low concentrations without any background interferences (the comparison of spectra obtained using Ag colloidal and dendritic nanoparticles, with highlighted position of the peak at 794 and 786 cm^{-1}, is displayed in Figure S37).

The histogram, plotting the count of spatially acquired spectra with certain Qi values for a concentration of emtricitabine 100,000 ng/ml, is shown in Figure 5A. The most of the spatially acquired spectra have a negligible emtricitabine enhancement. Shown in the histogram are the inner quartile distribution (centered not far from Qi = 0) and the top 10%, 5%, and 2%
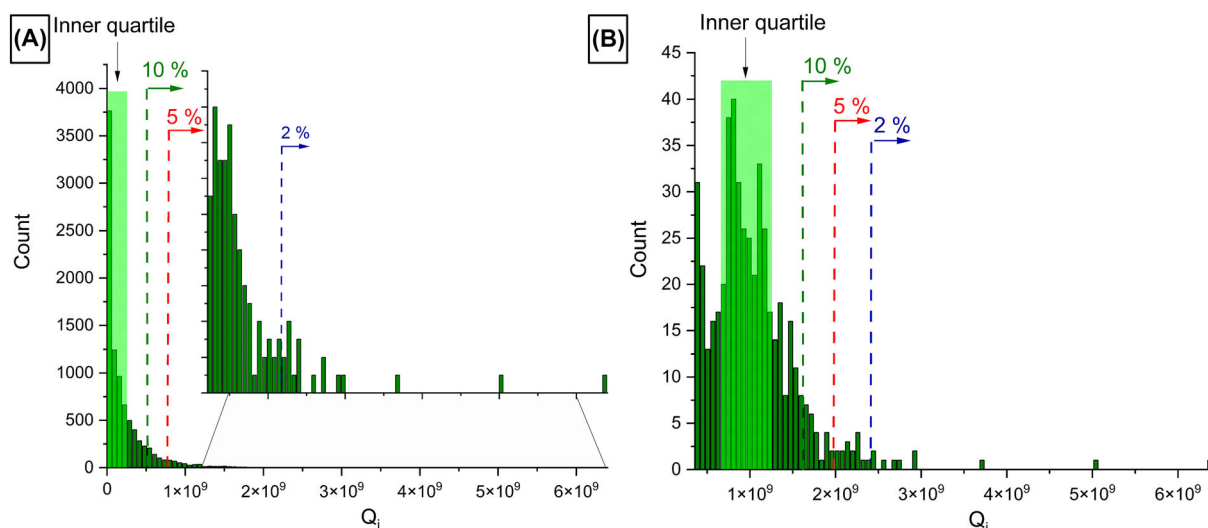
FIGURE 5 Histograms displaying the spectra count with specific Qi values calculated using (A) all and (B) the top 100 Qi-ranked spatially acquired spectra for the wells at a concentration of 100,000 ng/ml of emtricitabine using Ag dendrites nanoparticles. The inner quartile, the top 10%, 5%, and 2% distributions based on the Qi, are highlighted. For clarity, the inset enlarges the 2% distribution.
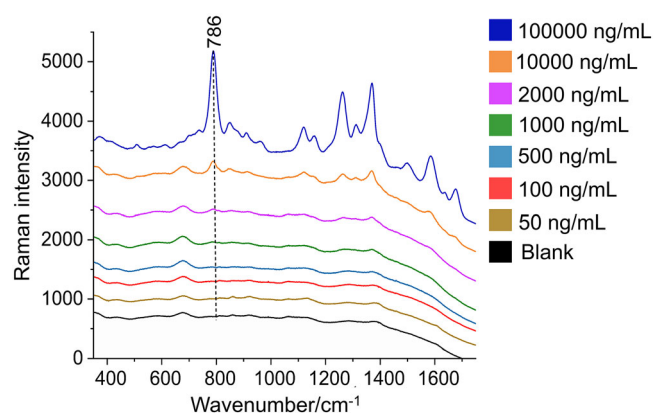

FIGURE 6 The average spectrum from five replicates for each measured concentration of emtricitabine was obtained using all spatially acquired spectra by using Ag dendrites nanoparticles (measured at the excitation wavelength with λ_{exc} = 785 nm and a laser power of 15 mW).
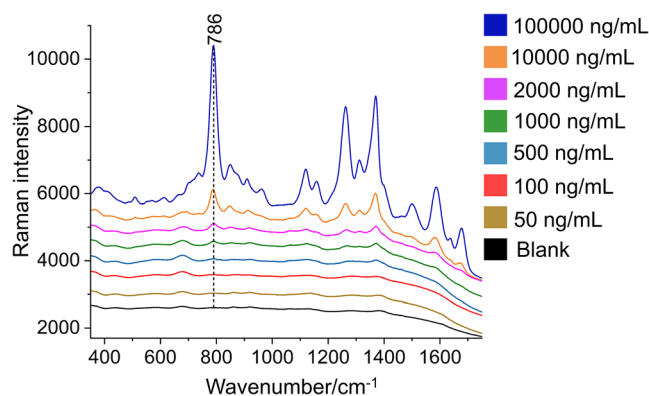

FIGURE 7 The average spectrum from five replicates for each measured concentration of emtricitabine was obtained using the top 100 highest Qi-ranked spatially acquired spectra from each well by using Ag dendrites nanoparticles (measured at the excitation wavelength with λ_{exc} = 785 nm and a laser power of 15 mW).

distributions as a function of the Qi. The extreme concavity of all the distributions is clearly indicative of a power law distribution. For the 2% distribution (Figure 5A inset), all the included spectra are in consistency with those with very high signal-to-noise ratios. Histograms using all spatially acquired spectra for concentrations of 10,000, 2,000, 1,000, and 500 ng/ml of emtricitabine are shown in Figures S38–S41. The histogram in Figure 5B is based on the top 100 Qi-ranked spatially acquired spectra from each well with concentration of emtricitabine 100,000 ng/ml. The trend of a power law of the distribution is slightly observable while passing the inner quartile distribution. Histograms using the top 100 Qi-ranked

spectra from each well with concentrations 10,000, 2,000, 1,000 and 500 ng/ml are shown in Figures S42–S45.

Both histograms demonstrate the extreme heterogeneity of the individual spectra, which is in agreement with findings from the data analysis of experiments with Ag colloidal nanoparticles. Looking at the top 2% of the distribution, which represents the best SERS enhancement, the spread of the Qi values is extremely large. Selecting the spectra with the high Qi values, the signal-to-noise ratios are greater as well as the fluctuation of the signal. With the selection of the spectra with high Qi values, both the signal-to-noise ratios and the fluctuation of the signal increase.
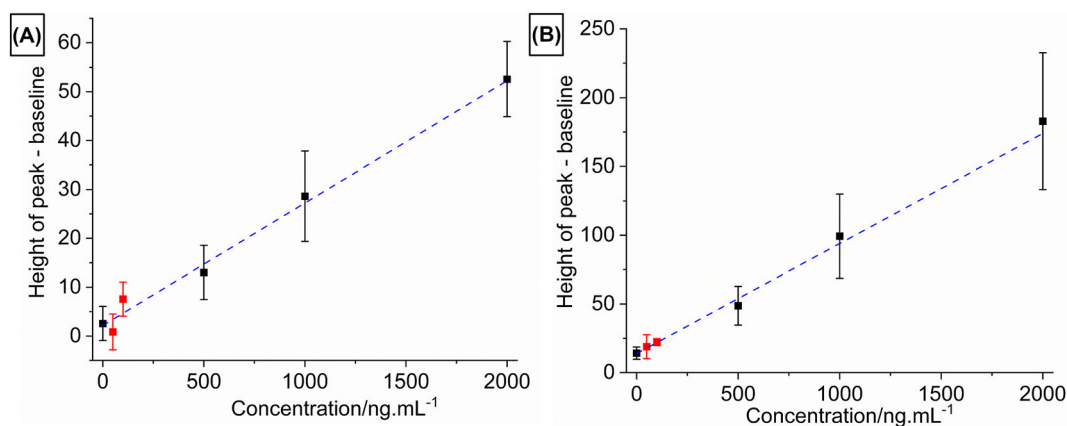
FIGURE 8 Calibration curves constructed based on the peak height at 786 cm^{-1} relative to the baseline calculated from the spectrum obtained using (A) all data and (B) the top 100 Qi-ranked spatially acquired data from each well. Error bars represent the standard deviation from each replicate. The calibration curves were fitted with a linear regression (blue dashed lines). The details about the fits are summarized in Table S10. The red points represent the values for 100 and 50 ng/ml, which were masked and there are not included in the linear fit.

Figure 6 shows the average of spatially acquired spectra as a function of the emtricitabine concentration. Each spectrum represents an average of all spatially acquired spectra for a given concentration. The spectra for concentrations 2,000, 1,000, 500, 100, and 50 ng/ml and blank are individually shown in Figures S46–S51 for clarity. As distinct from the use of Ag colloidal nanoparticles, the most intense emtricitabine peak at 786 cm^{-1} is prominent only down to concentration 500 ng/ml. For the concentrations below (i.e., 100 and 50 ng/ml), the peak is not clearly discerned from the blank. The extreme degree of heterogeneity of the spectral signal-to-noise is even more significant while using Ag dendrites nanoparticles and the need to select SERS spectra with high enhancement is even greater.

Contrary to this, Figure 7 shows spectra obtained by the spatial discrimination based on the Qi, where the top 100 Qi-ranked spatially acquired spectra from each well were included. The elimination of spectra from spatial positions that do not contain significant emtricitabine intensity, as represented by ranked Qi, results in a notable increase of signal to noise for most of the concentrations. This is consistent with the observations made using Ag colloidal nanoparticles. Nevertheless, the 786 cm^{-1} peak is only evident at 500 ng/ml concentrations, while for the lowest concentrations (i.e., 100 and 50 ng/ml), the spectra are comparable to blank. The individual spectra for 2,000, 1,000, 500, 100, and 50 ng/ml and blank are displayed in Figures S52–S57. Some spots were excluded due to the background highly influenced the intensity of the 786 cm^{-1} peak. Figures S58–S60 show spectra representing the top 10%, 5%, and 2% Qi distributions from the 100 highest Qi-ranked spectra for each well. The band assignment of the emtricitabine peaks with Ag colloidal and dendrites nanoparticles is summarized in Table S11.

The data sets using Ag dendrites nanoparticles were analyzed using the same approach as was used for Ag colloidal nanoparticles. Figure 8A shows a calibration curve built based on all, and Figure 8B the top 100 Qi-ranked spatially acquired data from each well. The calibration curves constructed using the top 10%, 5%, and 2% data of the top of 100 Qi-ranked data from each well are displayed in Figure S61–S63. For all calibration plots, error bars are included, showing the standard deviation of the average spectral intensity of the peak at 786 cm^{-1} in each of the five concentration wells along with a data point showing the mean result for the wells.

All calibration curves follow a very linear fit (R^2 greater than 0.99). In contrast, the error bars are almost overlapping in all the curves, despite the greater differences of the concentrations compared to the data sets shown in the previous section of the paper using Ag colloidal nanoparticles. In comparison to them, the Ag dendrites nanoparticles have a lower analytical sensitivity. However, in all cases, the use of the spatial discrimination results in a dramatic improvement in the analytical sensitivity (see Table S10). In the case of the Ag dendrites nanoparticles, the greater analytical sensitivity results in the elimination of the concentration error bar overlap for most instances, but the top 100 Qi-ranked discrimination represents the best overall compromise for the Ag dendrites nanoparticles.

4 | CONCLUSIONS

In this study, the data analysis approach using the Quality index (Qi) as a tool for sorting spatially acquired

spectra based on the intensity of the selected peak was introduced with the antiretroviral drug emtricitabine as the testing molecule, and its SERS spectral data sets were acquired by using two different silver nanoparticles: colloidal and dendritic. As could be expected, by the elimination of spectra from spatial positions that do not contain significant emtricitabine SERS intensity, results in a significant increase of signal to noise for most of the concentrations as well as a dramatic improvement of the slope of the calibration curves and therefore the analytical sensitivity (by $>5\times$) for both used nanoparticles. Nevertheless, the main advantage of this approach, which combines the collection of a large spectral dataset by using fully automatized PC-controlled scanning device and employing the Qi, represent a very cheap, easy, and time effective data analysis, which could be applied to a wide range of analytes by changing only a few parameters (e.g., the selection of a peak for Qi calculations).

Although in the current application, the scanning of each well involves the collection of large amounts of spectral data, with the use of the described low-cost scanning instrumentation, it is easy to implement a method that pre-scans wells at lower integration time and returns to hotspots for longer integration time analysis, thus providing faster analysis times along with higher signal-to-noise spectra.

The developed methodology followed by the data selection methods also lays the groundwork for applications with structurally similar molecules or drugs.[38] Moreover, part of the methodology and the data analysis process are currently being tested for the development of a clinically relevant assay using a simple matrix separation methodology to objectively the measure drug adherence.

ACKNOWLEDGMENTS

DATA AVAILABILITY STATEMENT

Data presented in this article are available on request from the corresponding author.

CONFLICT OF INTEREST

The authors declare no conflict of interest.

ETHICS STATEMENT

The submitting author declares that (i) the manuscript, or part of it, neither has been published nor is currently under consideration for publication by any other journal and that (ii) its publication is approved by all authors and tacitly or explicitly by the responsible authorities where the work was carried out and that, if accepted, it will not be published elsewhere in the same form, in English or in any other language, without the written consent of the copyright holder.

ORCID

Jana Hrncirova https://orcid.org/0009-0009-8540-6870
John B. Cooper https://orcid.org/0000-0001-9167-9589

REFERENCES

[1] UNAIDS, D. report **2021**.

[2] A. Temereanca, S. Ruta, *Front. Microbiol.* **2023**, *14*, 342.

[3] E. J. Arts, D. J. Hazuda, *Cold Spring Harb. Perspect. Med.* **2012**, *2*, 4.

[4] C. Flexner, *Nat. Rev. Drug Discov.* **2007**, *6*, 12.

[5] F. Amblard, D. Patel, E. Michailidis, S. J. Coats, M. Kasthuri, N. Biteau, Z. Tber, M. Ehteshami, R. F. Schinazi, *EJMECH* **2022**, *240*, 1.

[6] A. D. Holec, S. Mandal, P. K. Prathipati, C. J. Destache, *Curr. HIV Res.* **2017**, *15*(6), 411.

[7] L. M. Bang, L. J. Scott, *Drugs.* **2003**, *63*, 63.

[8] J. E. Frampton, C. M. Perry, *Drugs* **2005**, *65*, 1427.

[9] R. Smith, G. Villanueva, K. Probyn, Y. Sguassero, N. Ford, C. Orrell, K. Cohen, M. Chaplin, M. M. G. Leeflang, P. Hine, *CDSR* **2022**, *2022*, 7.

[10] P. P. Damulak, S. Ismail, R. Abdul Manaf, S. Mohd Said, et al., *IJRPH* **2021**, *18*, 5.

[11] S. Cîntă Pînzaru, I. Pavel, N. Leopold, W. Kiefer, *J. Raman Spectrosc.* **2004**, *35*(5), 35.

[12] R. Perez, A. Ruperez, J. Laserna, *Anal. Chim. Acta* **1998**, *376*, 2.

[13] H. Zhou, X. Li, L. Wang, Y. Liang, A. Jialading, Z. Wang, J. Zhang, *J. Rev. Anal. Chem.* **2021**, *40*, 1.

[14] R. Wang, K. Kim, N. Choi, X. Wang, J. Lee, J. H. Jeon, G. Rhie, J. Choo, *Sens. Actuators, B* **2018**, *270*, 270.

[15] C. Zanchi, L. Giuliani, A. Lucotti, M. Pistaffa, S. Trusso, F. Neri, M. Tommasini, P. M. Ossi, *Appl. Surf. Sci.* **2020**, *507*, 145109.

[16] L. A. Wali, K. K. Hasan, A. M. Alwan, *Spectrochim. Acta Part A.* **2019**, *206*, 206.

[17] L. He, M. Lin, H. Li, N. J. Kim, *J. Raman Spectrosc.* **2010**, *41*, 7.

[18] G. Fini, *J. Raman Spectrosc.* **2004**, *35*, 5.

[19] J. Cailletaud, C. de Bleye, E. Dumont, P.-Y. Sacré, L. Netchacovitch, Y. Gut, M. Boiret, Y.-M. Ginot, P. Hubert, E. Ziemons, *J. Pharm. Biomed. Anal.* **2018**, *147*, 147.

[20] H. Yilmaz, D. Yilmaz, I. C. Taskin, M. Culha, *Adv. Drug Delivery Rev.* **2022**, *184*, 114184.

[21] Y. S. Mary, M. Krátký, J. Vinsova, C. Baraldi, *J. Mol. Struct.* **2021**, *1245*, 131074.

[22] E. de Barros Santos, E. C. N. L. Lima, C. S. de Oliveira, F. A. Sigoli, *Anal. Methods* **2014**, *6*, 11.

[23] V. Burtsev, M. Erzina, O. Guselnikova, E. Miliutina, *Analyst* **2021**, *146*, 11.

[24] N. L. Rezk, R. D. Crutchley, A. D. Kashuba, *J. Chromatogr., B* **2005**, *822*, 822.

[25] A. Ramaswamy, A. S. A. G. Dhas, *Arabian J. Chem.* **2018**, *11*, 2.

[26] L. G. A. Borges, A. Savi, C. Teixeira, R. P. de Oliveira, M. L. F. de Camillis, R. Wickert, S. F. M. Brodt, T. F. Tonietto, R. Cremonese, L. S. da Silva, F. Gehm, E. S. Oliveira, J. H. D. Barth, J. G. Macari, C. D. de Barros, S. R. R. Vieira, *J. Crit. Care.* **2017**, *41*, 41.

[27] D. Doneva, M. Shishovska, Z. Mustafa, S. Memeti, K. Starkoska, S. Zulfikjari, A. Dimitrovska, Z. Arsova-Sarafinovska, *Maced Pharm. Bull.* **2022**, *68*, 1).

[28] P. Šimáková, M. Procházka, E. Kočišová, *J. Spectrosc.* **2012**, *27*, 27.

[29] M. Pucetaite, M. Velicka, J. Pilipavicius, A. Beganskiene, J. Ceponkus, V. Sablinskas, *J. Raman Spectrosc.* **2016**, *47*, 6.

[30] Y.-T. Kim, J. Schilling, S. L. Schweizer, G. Sauer, *Fundam. Appl.* **2017**, *25*, 25.

[31] R. Gao, H. Qian, C. Weng, X. Wang, *Sens. Actuators, B* **2020**, *321*, 128543.

[32] P. C. Lee, D. Meisel, *J. Phys. Chem.* **1982**, *86*, 86.

[33] N. Leopold, B. Lendl, *J. Phys. Chem. B.* **2003**, *107*, 24.

[34] J. A. Creighton, C. G. Blatchford, M. G. Albrecht, *J. Chem. Soc., Faraday Trans.* **1979**, *2*, 75.

[35] S. M. Heard, F. Grieser, C. G. Barraclough, J. V. Sanders, *J. Colloid Interface Sci.* **1983**, *93*, 93.

[36] J. Cooper, M. F. Abdelkader, K. Wise, Google Patents. **2013**.

[37] M. R. Butler, J. Hrncirova, T. A. Jacot, S. Dutta, M. R. Clark, J. B. Cooper, *Front. Nano.* **2023**, *5*, 5.

[38] J. Liu, Q. Lin, Y. Zhou, J. Dai, *Kona Powder Part. J.* **2020**, *37*, 2020004.

SUPPORTING INFORMATION

Additional supporting information can be found online in the Supporting Information section at the end of this article.

How to cite this article: J. Hrncirova, M. R. Butler, M. R. Clark, G. F. Doncel, J. B. Cooper, *J Raman Spectrosc* **2024**, 1. https://doi.org/10.1002/jrs.6721